Available online at www.sciencedirect.com
ScienceDirect
Combustion and Flame 147 (2006) 118–132
Combustion and Flame
www.elsevier.com/locate/combustflame

A computational study of an HCCI engine with direct injection during gas exchange

Haiyun Su [a], Alexander Vikhansky [a], Sebastian Mosbach [a], Markus Kraft [a,*], Amit Bhave [b], Kyoung-Oh Kim [c], Tatsuo Kobayashi [c], Fabian Mauss [d]

[a] *Department of Chemical Engineering, University of Cambridge, Cambridge CB2 3RA, United Kingdom*
[b] *Reaction Engineering Solutions Ltd., 61 Canterbury Street, Cambridge CB4 3QG, United Kingdom*
[c] *Higashifuji Technical Center, Toyota Motor Corporation, Mishuku 1200, Susono, Shizuoka 480-1193, Japan*
[d] *Division of Combustion Physics, Lund Institute of Technology, Box 118, S-22100 Lund, Sweden*

Received 4 October 2005; received in revised form 20 June 2006; accepted 3 July 2006

Available online 1 September 2006

Abstract

We present a new probability density function (PDF)-based computational model to simulate a homogeneous charge compression ignition (HCCI) engine with direct injection (DI) during gas exchange. This stochastic reactor model (SRM) accounts for the engine breathing process in addition to the closed-volume HCCI engine operation. A weighted-particle Monte Carlo method is used to solve the resulting PDF transport equation. While simulating the gas exchange, it is necessary to add a large number of stochastic particles to the ensemble due to the intake air and EGR streams as well as fuel injection, resulting in increased computational expense. Therefore, in this work we apply a down-sampling technique to reduce the number of stochastic particles, while conserving the statistical properties of the ensemble. In this method some of the most important statistical moments (e.g., concentration of the main chemical species and enthalpy) are conserved exactly, while other moments are conserved in a statistical sense. Detailed analysis demonstrates that the statistical error associated with the down-sampling algorithm is more sensitive to the number of particles than to the number of conserved species for the given operating conditions. For a full-cycle simulation this down-sampling procedure was observed to reduce the computational time by a factor of 8 as compared to the simulation without this strategy, while still maintaining the error within an acceptable limit. Following the detailed numerical investigation, the model, intended for volatile fuels only, is applied to simulate a two-stroke, naturally aspirated HCCI engine fueled with isooctane. The in-cylinder pressure and CO emissions predicted by the model agree reasonably well with the measured profiles. In addition, the new model is applied to estimate the influence of engine operating parameters such as the relative air–fuel ratio and early direct injection timing on HCCI combustion and emissions. The qualitative trends observed in the parametric variation study match well with experimental data in literature.

Keywords: HCCI; SRM; Direct injection

* Corresponding author.
E-mail address: mk306@cam.ac.uk (M. Kraft).

0010-2180/$ – see front matter
doi:10.1016/j.combustflame.2006.07.005

1. Introduction

The development of efficient internal combustion engines with ultralow emissions is necessitated by strict regulations on exhaust gas composition and fuel economy. Homogeneous charge compression ignition (HCCI) technology, incorporating the advantages of both spark ignition and compression ignition, is a potential candidate for future ultralow-emission engine strategies. There are, however, technical hurdles to overcome before large-scale production and application of HCCI engines can be achieved. Further research and development needs to be conducted in order to control HCCI combustion and expand the engine operating window. Various approaches such as multiple direct injections, variable valve timing, dual fuels, variable compression ratio, and intake charge heating have shown potential to tackle the above mentioned issues [1].

In particular, direct injection (DI) has been widely investigated to control the spontaneous combustion as well as to expand the engine operating region. Optimum values for single direct injection timings have been demonstrated under different operating load conditions, and have been shown to be capable of expanding the lean limit by promoting better fuel ignitability [2,3]. Early injection timing results in a more homogeneous mixture, and it can lead to thermodynamically unfavorable advanced combustion timing under high load [4,5]. To help control ignition timing and combustion duration, a dual-injection strategy has been investigated [4,6]. The second fuel injection can function as an ignition trigger and can help to limit pressure rise rates caused by too rapid combustion. Elsewhere, to increase the mixing efficiency and expand the operation limit, a number of methods were studied to control the direct injection procedure, such as varying injection pressure, spray angle, spray shape, and using impingement spray [7–11]. Furthermore, Su et al. [12] have evaluated the effects of pulse injection modes on the suppression of wall wetting.

To evaluate these strategies, computational modeling tools can provide significant insight in a cost- and time-effective manner. A combined single-zone and multizone based engine cycle model has been introduced for modeling early DI HCCI operation [13]. In their subsequent study, this approach was further improved by incorporating a refined grid to resolve the early spray evolution and a coarse grid when chemical kinetics became prominent [14]. In another study, the influence of air–fuel distribution and temperature distribution on the ignition dwell in an early DI HCCI engine has been modeled using a KIVA 3V code [15]. It was demonstrated that, at the end of fuel injection, the ignition dwell duration was more sensitive to the in-cylinder temperature distribution than the air–fuel distribution. However, these modeling approaches have been limited to early direct injection, and further development for modeling multiple injection and late direct injection HCCI is required.

Probability density function (PDF)-based models provide a sophisticated approach while including detailed chemistry and accounting for inhomogeneities in composition and temperature. As special cases, stochastic reactor models (SRMs) are derived from the PDF transport equations assuming statistical homogeneity. The closed volume SRM has been demonstrated to accurately predict autoignition timing, in-cylinder pressure, and emissions in HCCI engines [16–18]. The model has also been coupled with a commercial code to enable multiple engine cycle simulation [19,20]. In previous works, the SRM has been applied to simulate port-fuel-injected HCCI engines. The present work is the first step of development of an advanced SRM-DI model capable of simulating multiple direct injection HCCI combustion and emissions. This advancement entails the modeling of the engine breathing processes in the existing SRM framework, thus accounting for the detailed chemical kinetics, particularly during multiple and late direct injections.

The *aims of this paper* are the following:

(1) To develop a new SRM-DI to account for gas exchange and compression–combustion–expansion in a direct injection HCCI engine, such that detailed chemistry can be accounted for during the direct injection process.
(2) To formulate a weighted-particle Monte Carlo method to solve the transport equation including the gas exchange terms. As compared to the equiweighted method used in previous works [18–20], a weighted-particle method requires fewer particles to account for the gas exchange process.
(3) To incorporate a novel down-sampling algorithm to reduce the number of particles in the ensemble [21]. A number of new particles are added into the system during the air intake and fuel injection, which results in a dramatic increase in the computational cost for the following cycle. In this work, a down-sampling algorithm is employed to reduce the number of particles while conserving the most important statistical properties of the ensemble.
(4) To validate the new model against the experimental data for in-cylinder pressure profile and emissions at a single engine operation point.
(5) To apply the new SRM-DI to predict the qualitative trends associated with some engine parametric variation, such as varying air–fuel ratio and

early DI timing to test the capability of the model to simulate early DI HCCI engines.

This paper is organized as follows. In the second section, the submodels for the DI HCCI engine are described. In Section 3, the numerical method and its implementation are presented. In Section 4, an error analysis is conducted to determine appropriate down-sampling parameters by studying the statistical errors associated with the procedure. Multiple cycle simulations were performed to test if the error due to down-sampling was accumulated in subsequent engine cycles. Furthermore, the effect of the down-sampling procedure in terms of computational gains and accuracy are evaluated by comparing the in-cylinder temperature and chemical species obtained with and without this technique. Two cases, "well-mixed" and "partially mixed," are investigated. After understanding its numerical behavior, the model was validated (Section 5) against experimental data from a two-stroke DI HCCI engine. In Section 6, the SRM-DI is applied to study the effects of varying air–fuel equivalence ratio and early direct injection timing on the combustion and emissions. Conclusions are drawn in the final section and future work is discussed.

2. SRM for direct injection HCCI

The partially stirred reactor (PaSR) model has been widely used as a test bed for evaluating chemical mechanisms and mixing schemes in the field of combustion [22–24]. This model assumes statistical homogeneity of the mixture in the reactor. It accounts for mixing and can include large coupled chemical reaction mechanisms.

In this study, we develop a stochastic reactor model on the basis of the PaSR to simulate a direct injection HCCI engine. Early DI HCCI, as the name suggests, involves an early injection of fuel into a mixture of air and trapped residual gas (TRG), followed by compression and autoignition. This model is referred to as the stochastic reactor model for direct injection (SRM-DI) and can be written as

$$\begin{aligned}
&\frac{\partial}{\partial t}\mathcal{F}(\psi,t)+\underbrace{\frac{1}{V}\frac{\mathrm{d}V}{\mathrm{d}t}\mathcal{F}(\psi,t)}_{\text{piston movement}}\\
&+\underbrace{\sum_{i=1}^{s+1}\frac{\partial}{\partial\psi_i}\big[G_i(\psi)\mathcal{F}(\psi,t)\big]}_{\text{chemical kinetics}}\\
&+\underbrace{\frac{1}{h}\big[U(\psi_{s+1}+h)\mathcal{F}(\psi_1,\ldots,\psi_s,\psi_{s+1}+h,t)-\underbrace{U(\psi_{s+1})\mathcal{F}(\psi,t)\big]}_{\text{convective heat transfer}}}_{\text{convective heat transfer}}\\
&=\underbrace{\sum_{i=1}^{s+1}\frac{\partial}{\partial\psi_i}\left[\frac{C_\phi}{2\tau_{\mathrm{m}}}\big(\psi(t)-\langle\psi_i\rangle\big)\mathcal{F}(\psi,t)\right]}_{\text{mixing}}\\
&+\underbrace{\frac{{}^{\mathrm{a}}\mathcal{F}_{\mathrm{in}}(\psi,t)}{\tau_{\mathrm{a}}}-\frac{\mathcal{F}(\psi,t)}{\tau_{\mathrm{e}}}+\frac{{}^{\mathrm{f}}\mathcal{F}_{\mathrm{in}}(\psi,t)}{\tau_{\mathrm{f}}}}_{\text{gas exchange and fuel injection}} \qquad (1)
\end{aligned}$$

with the initial condition

$$\mathcal{F}(\psi,0)=\mathcal{F}_0(\psi), \qquad (2)$$

where $\mathcal{F}$ is the mass density function (MDF) and ψ stands for scalar variables such as mass fractions of chemical species and temperature; i.e., $\psi=(\psi_1,\ldots,\psi_s,\psi_{s+1})=(Y_1,\ldots,Y_s,T)$. The five terms accounting for piston movement, chemical kinetics and volume change, convective heat transfer, mixing, and gas exchange and fuel injection, respectively (as indicated in Eq. (1)) are now described in more detail.

The second term on the left-hand side (LHS) of Eq. (1) denotes the effect of the piston movement on the MDF. The chemical kinetics and the energy associated with the change in volume is represented by the third term on the LHS, where

$$G_i=\frac{M_i\dot{\omega}_i}{\rho},\quad i=1,\ldots,s, \qquad (3)$$

$$G_{s+1}=-\frac{1}{\rho c_{\mathrm{v}}}\sum_{i=1}^{s}e_iM_i\dot{\omega}_i-\frac{p}{mc_{\mathrm{v}}}\frac{\mathrm{d}V}{\mathrm{d}t}. \qquad (4)$$

Here, M_i is the molar mass of species i, ρ is the density of the mixture, $\dot{\omega}_i$ is the molar production rate of the ith species, V is the volume, m is the mass, and e_i represents the specific internal energy of species i. In this paper, a deterministic solver based on a backward differentiation formula method was implemented to solve the set of stiff ordinary differential equations.

The fourth term on the LHS of Eq. (1) represents the heat transfer model, where h denotes the fluctuation (the implementation is discussed in Section 3.1)

$$U(T)=-\frac{h_{\mathrm{g}}A}{c_{\mathrm{v}}M_{\mathrm{tot}}}(T-T_{\mathrm{W}}), \qquad (5)$$

h_{g} is the Woschni heat transfer coefficient, A is the heat transfer area, M_{tot} is the total mass, c_{v} is the specific heat capacity at constant volume, and T_{W} denotes the wall temperature. The convective heat transfer occurring between the fluid and the wall is modeled as a stochastic jump process based on the Woschni heat transfer coefficient [18,20].

For mixing, the interaction by exchange with the mean (IEM) model, represented by the first term on

the right-hand side (RHS) of Eq. (1), was used. The IEM model (also known as the linear mean square estimation (LMSE) model) is a deterministic model that works on the principle that the scalar value at a point approaches the mean scalar value over the entire volume with a characteristic time τ_m. For a single scalar, the IEM model is given by

$$\frac{d\psi(t)}{dt} = -\frac{C_\phi}{2\tau_m}\big(\psi(t) - \langle\phi\rangle\big), \tag{6}$$

where C_ϕ is a model constant. In this paper, C_ϕ is set to 2.0 as suggested by Pope [25].

On the RHS of Eq. (1), the last three terms account for the gas exchange and fuel injection processes in a DI HCCI (air intake, exhaust, and fuel injection). τ_a, τ_e, and τ_f denote the characteristic residence times of air, exhaust gas, and fuel, respectively. ${}_a\mathcal{F}_{in}$, ${}_f\mathcal{F}_{in}$ stand for the mass density functions associated with the intake air and fuel streams.

3. Numerical method

In this section, the numerical method employed for the solution of Eq. (1) is discussed in detail. A weighted-particle Monte Carlo method with an operator splitting procedure has been implemented in this work.

The particle method involves representation of the reactive system by a notional ensemble of N particles. Thus the approximation for the mass density function $\mathcal{F}$ reads

$$\begin{aligned}\mathcal{F}(\psi,t) &= \rho(\psi,t) f(\psi,t)\\ &\approx \frac{\rho(\psi,t)}{\sum_{i=1}^{N} W^{(i)}} \sum_{i=1}^{N} W^{(i)} \delta\big(\psi - \psi^{(i)}(t)\big)\\ &= \frac{1}{V(t)} \sum_{i=1}^{N} W^{(i)} \delta\big(\psi - \psi^{(i)}(t)\big),\end{aligned} \tag{7}$$

where $W^{(i)}$ is the statistical weight of the ith particle.

Therefore,

$$\begin{aligned}\big\langle\rho(t)\big\rangle &= \int \rho(\psi,t) f(\psi,t)\, d\psi = \int \mathcal{F}(\psi,t)\, d\psi\\ &\approx \frac{1}{V(t)} \sum_{i=1}^{N} W^{(i)} = \frac{M_{tot}}{V(t)}.\end{aligned} \tag{8}$$

Following this approximation, $\mathcal{F}_0(\psi) \approx \frac{1}{V_0} \times \sum_{i=1}^{N} W_0^{(i)} \delta(\psi - \psi_0^{(i)})$, each particle is moved according to the evolution of the mass density function as given in Eq. (1).

An operator splitting technique is used to simplify an evolution equation by splitting the complex equation into a set of equations. The advantage is that the split equations can be treated separately at the expense of introducing a splitting error. The operator splitting technique has been discussed in detail elsewhere [26] and has been applied to the PDF transport equation by Pope [25]. It has been demonstrated that the splitting is first-order accurate [27].

In previous work [18–20], an equiweighted particle method was used. In this work, a weighted-particle method is employed so that it can be directly coupled with the down-sampling procedure. The implementation of the chemical kinetics, mixing, and heat transfer submodels is readily generalized to weighted-particle systems, since they are independent of the statistical weight.

3.1. Implementation of SRM-DI

Based on the numerical method described above, the SRM-DI was implemented as follows:

(1) Initialize $t = 0, t_{stop}, \Delta t$, CAD (crank angle degree) = IVC (intake valve closing). Determine the state of the particle system at time $t = 0$.
(2) Progress in time with a time step, $t \mapsto t + \Delta t$. If $t > t_{stop}$, then stop. Else, if CAD < EVO (exhaust valve opening) go to step (3); otherwise go to step (8).
(3) Perform the mixing step: the particle ensemble is updated according to Eq. (6).
(4) Perform the reaction step.
(5) Perform the mixing step.
(6) Choose particles uniformly and perform the heat transfer step $T^{(i)} \mapsto T^{(i)} - h^{(i)}$, where the fluctuation $h^{(i)} = \frac{T^{(i)} - T_W}{C_h}$ and C_h is a parameter in the model that determines the magnitude of the fluctuation.
(7) Go to step (2).
(8) Perform the inflow–outflow step, as described below.
(9) If CAD = IVC perform the down-sampling.
(10) Go to step (2).

The inflow–outflow step as given in point (8) above is a new submodel and is discussed in detail in the next section.

3.2. Implementation of inflow and outflow

In this study, the inflow–outflow model accounts for the following events: intake of fresh air, fuel injection, and exhaust.

In an inflow event, fresh air and fuel particles are added to the system, $N \mapsto N + N_{in}$, where N_{in} denotes the number of new particles added per step (Δt). The weight of a new particle equals its mass,

leading to

$$W^{(i)} = \frac{\frac{\Delta t}{\tau_{\text{in}} \times M_{\text{tot}}}}{N_{\text{in}}} = \frac{\dot{m}^{\text{in}} \times \Delta t}{N_{\text{in}}}, \quad i = N+1, \ldots, N+N_{\text{in}}. \tag{9}$$

Here, τ_{in} is the characteristic residence time of the inflow stream (e.g., air, fuel), and $\dot{m}^{\text{in}}$ denotes the mass flow rate of the inflow stream.

For outflow we note that the mass to be removed during the time interval Δt is given by $\Delta t \dot{m}_{\text{e}}^{\text{out}}$, where $\dot{m}_{\text{e}}^{\text{out}}$ denotes the mass flow rate of the exhaust stream. Hence, the fraction of the mass to be removed equals $\Delta t \frac{\dot{m}_{\text{e}}^{\text{out}}}{M_{\text{tot}}}$. Furthermore, in the experimental studies on the two-stroke HCCI test engine, it was observed that less than 1% of fuel was lost on account of the fuel injection during the outflow event. Therefore, only the weights of the stochastic particles associated with the exhaust (residual burnt gases) are reduced during an outflow event. However, due to mixing of a small amount of fresh fuel with the outflow, some fuel is lost through the exhaust.

For the particles associated with the exhaust, the weight is reduced as follows:

$$W^{(i)} \mapsto W^{(i)} \times \left(1 - \frac{\Delta t}{\tau_{\text{e}}}\right) = W^{(i)} \times \left(1 - \Delta t \frac{\dot{m}_{\text{e}}^{\text{out}}}{M_{\text{tot}}}\right), \quad i = 1, \ldots, N. \tag{10}$$

For simplicity, we assume constant inflow and outflow rates throughout. Within a time step $t \leqslant \text{CAD} \leqslant t + \Delta t$ the algorithm is implemented as follows:

(1) Given the state at CAD = EVO, initialize $W^{(i)} = W_0^{(i)}$.
(2) For EVO < CAD $\leqslant$ EVC (exhaust valve closing), perform an outflow event; i.e., reduce the particle weight $W^{(i)}$ proportionally according to (10).
(3) For IVO (intake valve opening) < CAD $\leqslant$ IVC, perform the inflow of fresh air; i.e., add N_{a} particles to the ensemble according to Eq. (9), where $\dot{m}_{\text{in}} = \dot{m}_{\text{air}}^{\text{in}}$ and $N_{\text{in}} = N_{\text{a}}$. $\dot{m}_{\text{air}}^{\text{in}}$ denotes the mass flow rate of inflowing air.
(4) For SOI (start of injection) < CAD $\leqslant$ EOI (end of injection), perform the inflow event for fuel streams according to Eq. (9) with $\dot{m}_{\text{in}} = \dot{m}_{\text{fuel}}^{\text{in}}$ and $N_{\text{in}} = N_{\text{f}}$. $\dot{m}_{\text{fuel}}^{\text{in}}$ denotes the mass flow rate of injected fuel.

Adding particles to the ensemble causes a significant increase in computational expense. It is necessary to reduce the number of the particles without affecting the statistics of the ensemble. This procedure, called down-sampling, is discussed in the next section.

3.3. Down-sampling algorithm

The simplest method, which removes particles chosen according to uniform distribution from the ensemble, leads to large spurious fluctuations of energy and mass of the chemical species. In this study we apply the method introduced by Vikhansky and Kraft [21], which randomly redistributes the statistical weights between the particles in such a way that the weight of some particles becomes 0 (i.e., the particles are removed), while the most important statistical moments of the ensemble are conserved and overall the ensemble remains statistically unaffected (a more detailed description of the method is given in Ref. [21]). In the present investigation we chose ns species, which, due to their high significance, have to be conserved exactly in addition to conserving the enthalpy of the mixture. The algorithm is implemented as follows:

(1) Determine the state of the particle system at the time corresponding to IVC:
$$\psi_j^{(i)}, \quad W^{(i)}, \quad t = \text{IVC}, \quad i = 1, \ldots, N, \ j = 1, \ldots, s+1.$$
(2) Calculate the average values of all properties $\langle \psi_j \rangle$ and sort them in descending order, where
$$\langle \psi_j \rangle = \frac{\sum_{i=1}^{N} \psi_j^{(i)} \times W^{(i)}}{\sum_{i=1}^{N} W^{(i)}}, \quad i = 1, \ldots, N, \ j = 1, \ldots, s+1.$$
(3) Choose the first ns species according to $\langle \psi_j \rangle$ and the enthalpy; then calculate the $(N \times (ns+1))$ matrix Π, where
$$\Pi_{ji} = \psi_j^{(i)}, \quad i = 1, \ldots, N, \ j = 1, \ldots, ns+1.$$
(4) Set maximum weight $W_{\max}$ and perform the reduction (for the reduction algorithm see [21]) with parameters Π and $W_{\max}$. Calculate the new statistical weight $W^{(i)}$.
(5) Remove all particles satisfying the condition $W^{(i)} < \sum W^{(i)} \times 10^{-5}$. The number of remaining particles n lies in the interval $(\frac{\sum W^{(i)}}{W_{\max}}, \frac{\sum W^{(i)}}{W_{\max}} + ns + 1)$.

4. Numerical properties of the algorithm

The SRM-DI discussed above was implemented to simulate a two-stroke, three-cylinder, isooctane fueled HCCI test engine. The model was applied to

Table 1
Engine operating parameters

Description	Value	Units
Displaced volume	1500	cm^3
Bore	86	mm
Stroke	86	mm
Connection rod	154	mm
Speed	1200	RPM
Fuel	Isooctane	–
Compression ratio	13.5	–
EVO/EVC	140/180 ATDC	CAD
IVO/IVC	155/215 ATDC	CAD
SOI/EOI	165/175 ATDC	CAD

simulate only the first cylinder operating in the HCCI mode. An isooctane and n-heptane reaction mechanism consisting of 157 species and 1552 reactions was used to simulate the fuel chemistry [19]. The description of the engine and its operating parameters is given in Table 1. In the study, the temperature and the mass fractions of OH, CO, and NO_x were considered to represent the scalar variables to be studied for data analysis. Two cases of turbulent mixing, one partially mixed ($\tau_m = 2.0 \times 10^{-2}$ s) and the other well mixed ($\tau_m = 2.0 \times 10^{-4}$ s), were chosen to represent the extremes of the average characteristic mixing times from EVO to IVC. The mixing time for compression–combustion–expansion is set to $\tau_m = 1.0 \times 10^{-2}$ s, as the turbulence time scale is on the order of 10^{-2} s around TDC [16]. Furthermore, for all the cases studied, the mixing time during the outflow (10) event is set to 2.0×10^{-1} s to maintain the loss of fresh air charge and fuel through the exhaust below 1%. However, the duration of engine scavenging after EVC is sufficient to make the charge almost homogeneous at IVC. Before investigating the numerical properties of the down-sampling algorithm, the influence of the number of fuel particles added to the system during every step of the direct injection phase was studied. It was found that the simulated results obtained by varying the numbers of fuel particles agreed well with the case where only one fuel particle was added per time step. This indicates that for the given operating conditions, the change in number of inflowing fuel particles does not influence the model predictions significantly. Next, we evaluate the sensitivity of the down-sampling technique to its parameters.

4.1. Determination of down-sampling parameters

The down-sampling algorithm contains two parameters, the number of conserved scalars $ns + 1$ and the number of particles n. In this section, the influence of these parameters on the statistical and systematic errors is studied and then the appropriate down-sampling parameters are determined. In order to study the error incurred exclusively by the down-sampling process, the stochastic heat transfer submodel was switched off. Thus, the down-sampling procedure is the sole source of statistical error. Furthermore, the partially mixed case was studied particularly due to its high standard deviation.

In the particle method, the macroscopic properties are calculated by averaging over all particles at each point in time. In order to estimate the random fluctuations of the down-sampling algorithm, L repetitions were performed. The corresponding values of the macroscopic properties are denoted by $\zeta^{(n,1)}(t), \ldots, \zeta^{(n,L)}(t)$, where n is the number of particles after down-sampling.

The empirical mean value of the macroscopic properties is

$$\eta_1^{(n,L)}(t) = \frac{1}{L}\sum_{l=1}^{L} \zeta^{(n,l)}(t),$$

and the empirical variance of the macroscopic properties is

$$\eta_2^{(n,L)}(t) = \frac{1}{L}\sum_{l=1}^{L} \big[\zeta^{(n,l)}(t)\big]^2 - \big[\eta_1^{(n,L)}(t)\big]^2.$$

The statistical error is the difference between the empirical mean value and the expected value of the macroscopic properties. The statistical error is defined as

$$C_{\text{stat}} = \max_i \left\{ \alpha_p \sqrt{\frac{\eta_2^{(n,L)}(t_i)}{L}} \right\},$$
$$t_i \leqslant t_{\text{stop}},\ t_i = i\,\Delta t,\ i \geqslant 0,$$

where $\alpha_p = 3.29$ is used for a confidence level of $p = 0.999$.

The systematic error is the difference between the expectation of the macroscopic properties and the exact value of the functional. In this study, the base case, i.e., the simulation without down-sampling, is used as the reference solution $F(t)$. Thus, a measure of the systematic error is defined as

$$C_{\text{sys}} = \max_i \big\{ \big| \eta_1^{(n,L)}(t_i) - F(t_i) \big| \big\}.$$

Asymptotically (i.e., for $L \to \infty$), the statistical error is inversely proportional to $\sqrt{L}$. To determine an appropriate number of repetitions, two set of simulations, one with 10 and the other with 80 repetitions, were compared. For these two cases 10 species were conserved. A detailed comparison is given in Table 2. From Table 2, it can be observed that the statistical error scales inversely to $\sqrt{L}$ and the error is sufficiently small at $L = 10$ to keep the number of repetitions at that value in the remainder of this section.

Table 2
Comparison of statistical errors between the sets of simulation with $L = 10$ and $L = 80$ (OH, CO, NO_x are expressed in terms of mass fraction)

	OH	CO	NO_x	T [K]
$L_1 = 10$	6.16×10^{-8}	2.45×10^{-4}	1.29×10^{-9}	6.36
$L_2 = 80$	2.21×10^{-8}	8.62×10^{-5}	5.58×10^{-10}	2.22
$\frac{C_{\text{stat}}^{L_1}}{C_{\text{stat}}^{L_2}} \times \frac{\sqrt{L_1}}{\sqrt{L_2}}$	0.985	1.0	0.817	1.01

Table 3
Comparison of statistical errors and systematic errors (OH, CO, NO_x are expressed in terms of mass fraction)

	OH	CO	NO_x	T [K]
		$ns = 10, n = 32$		
C_{stat}	8.98×10^{-8}	3.31×10^{-4}	2.14×10^{-9}	9.22
C_{sys}	6.55×10^{-8}	7.49×10^{-5}	1.25×10^{-9}	2.53
		$ns = 10, n = 213$		
C_{stat}	1.01×10^{-8}	1.09×10^{-4}	3.56×10^{-10}	1.62
C_{sys}	7.15×10^{-9}	2.31×10^{-5}	3.82×10^{-10}	0.66

In Table 3, the systematic and the statistical errors for the number of particles, $n = 32$ and $n = 213$ are provided. These data indicate that the statistical error is generally larger than the systematic error. Therefore, in the next part we will only focus on the statistical error.

Next, we conducted a series of six simulations. In cases (a) to (d), 9, 19, 39, and 79 species were conserved respectively. Case (e) denotes the simulation run conserving just the four elements (C, H, O, N). In all the cases the total enthalpy was conserved, while the number of particles after down-sampling varied from 13 to 233. Case (f) was performed without conserving any properties and the number of particles was varied as 10, 20, 45, 95, and 200. The comparison of statistical errors associated with the species OH, CO, NO_x, and the temperature T between these simulations is shown in Fig. 1. It can be observed that the statistical error for OH, NO_x, and T scales inversely with the number of particles, whereas that for CO is inversely proportional to $\sqrt{n}$. This difference could arise from the correlation of the scalar properties for different particles. Furthermore, the number of conserved species were not found to influence the error significantly. However, without conserving any species, a significant error was incurred. Based on this study, it can be concluded that for the engine simulation with the given conditions, case (a) conserving 9 species with 50 particles retains adequate accuracy. Having studied the down-sampling parameters, we now consider multiple engine cycle simulations. Cycle simulations help in better understanding cyclic variation of the scalar properties and thereby devising variable control strategies for optimal engine performance and emissions.

4.2. Multiple cycle simulation

In this section multicycle simulations are conducted to investigate the accumulation of error on account of the down-sampling during several engine cycles. Here, ns and n are set to 19 and 120, respectively. With the down-sampling strategy implemented, 10 successive engine cycles for both cases of characteristic mixing times were simulated. A confidence band, with respect to the number of particles, for the simulation with one repetition was employed for data analysis.

The empirical mean value of scalar variables, in a single-run simulation, is

$$\eta_1^n(t) = \frac{\sum_{i=1}^n \psi^{(i)}(t) W^{(i)}}{\sum_{i=1}^n W^{(i)}},$$

where n represents the number of particles after down-sampling.

The empirical variance is

$$\eta_2^n(t) = \frac{\sum_{i=1}^n [\psi^{(i)}(t)]^2 W^{(i)}}{\sum_{i=1}^n W^{(i)}} - \left[\eta_1^n(t)\right]^2.$$

We use as an estimate for the variation of the empirical mean the confidence interval

$$I_{\text{p}} = \left[\eta_1^n(t) - 3.0\sqrt{\frac{\eta_2^n(t)}{n}}, \eta_1^n(t) + 3.0\sqrt{\frac{\eta_2^n(t)}{n}} \right]. \tag{11}$$

Fig. 2 depicts the effect of down-sampling on mass fractions of CO and NO_x for the partially mixed case, while Fig. 3a shows mass fractions of NO_x for the well-mixed case. In these figures "c" denotes the engine cycle index. For the partially mixed case the confidence band for the 10th cycle for the chemical species (Fig. 2) are very wide, indicating a large standard deviation (the same situation for other cycles). This is due to the fact that the inhomogeneities are very strong because of slow mixing. As compared to the partially mixed system, the simulation results for the well-mixed system show a much narrower confidence band on account of the greater homogeneity and hence lower standard deviation. Furthermore, for the well-mixed system, the temperature and mass fractions of OH and CO from the third to the 9th cycles lie within the confidence bands of the 10th cycle. However, the profile for the NO_x mass fraction lies outside the confidence band of the last cycle. For example, from Fig. 3b, it can be seen that the NO_x confidence band of the 10th cycle does not

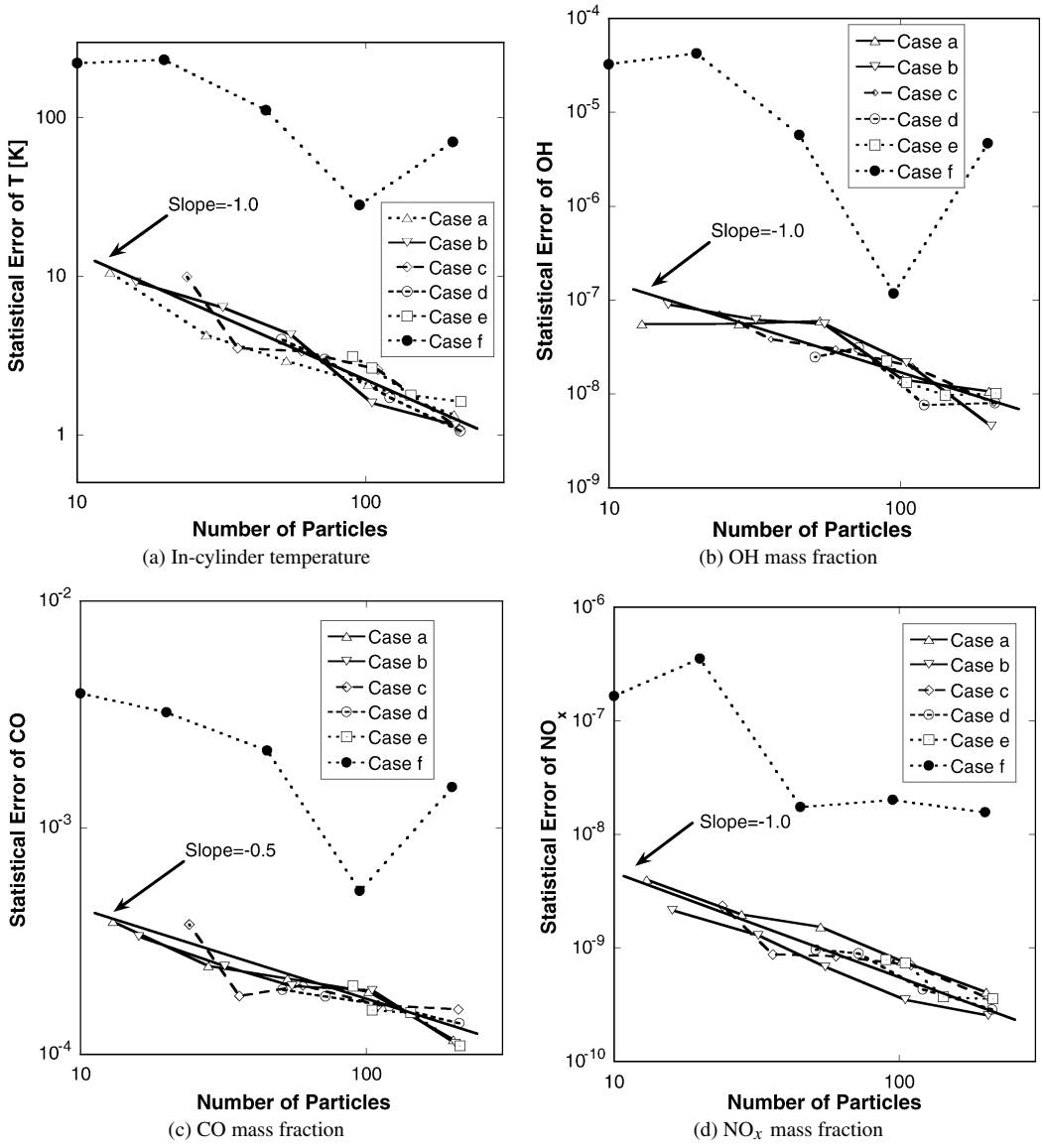

(a) In-cylinder temperature (b) OH mass fraction

(c) CO mass fraction (d) NO_x mass fraction

Fig. 1. Effect of the number of conserved species and the number of particles after down-sampling on the statistical errors of the mixture's properties in the partially mixed case: (a) in-cylinder temperature, (b) OH mass fraction, (c) CO mass fraction, (d) NO_x mass fraction.

overlap with those from the 6th and 7th cycles. This means that the mixture is so well mixed that the variance of mean NO_x mass fraction is on the same order as its cycle-to-cycle variation. This is due to its high sensitivity to the temperature fluctuations in the system. However, there is no evidence for accumulated error with respect to the number of cycles.

In conclusion, for both the well-mixed and partially mixed cases, the down-sampling did not accumulate noticeable errors for the multicycle simulations.

4.3. Down-sampling: efficiency gains

In order to evaluate the effect of incorporating the down-sampling algorithm into the SRM-DI model, the simulation results obtained with and without down-sampling were compared. The influence on the computational expense and the error caused by down-sampling for the partially mixed and well-mixed systems were also studied. For this study, we define the *down-sampling factor* M as the particle reduction ratio, i.e., $M := N/n$, where N and n are the number of particles before and after down-sampling, respec-

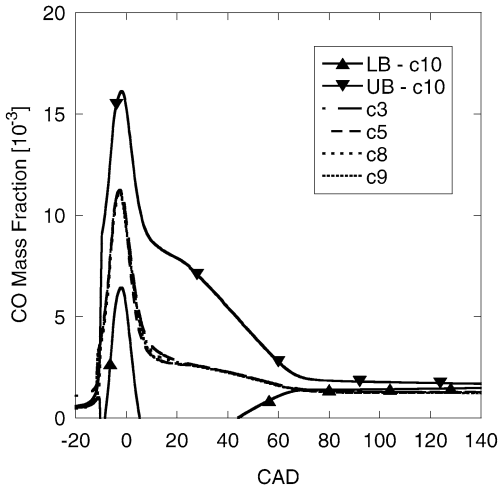

(a) CO mass fraction

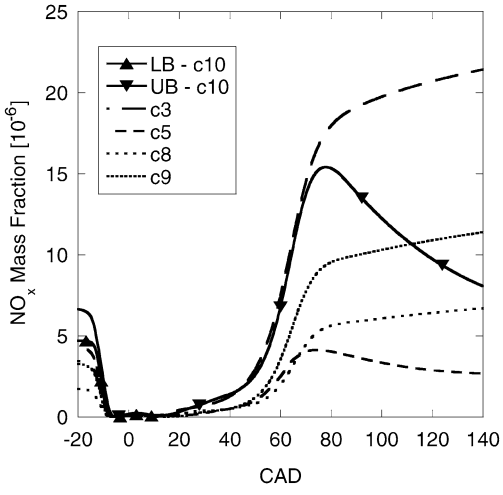

(b) NO_x mass fraction

Fig. 2. Mean properties of the mixture for several engine cycles (confidence bands plotted for the 10th cycle) in the partially mixed case. Here, "c" denotes the engine cycle index: (a) CO mass fraction; (b) NO_x mass fraction.

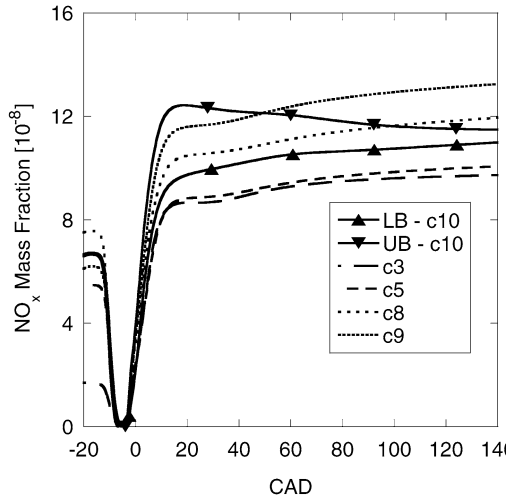

(a) Mean value

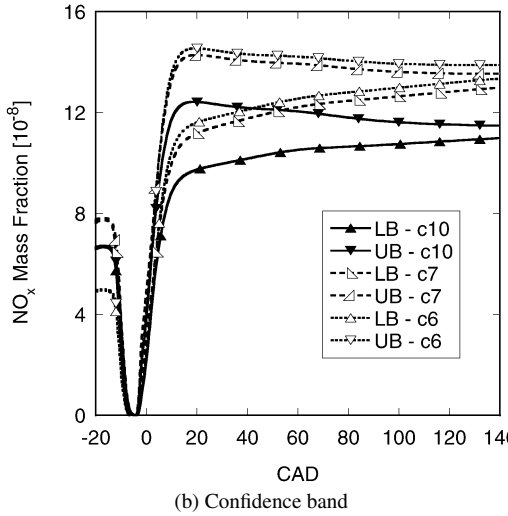

(b) Confidence band

Fig. 3. Mean NO_x mass fraction and the confidence band for several engine cycles (confidence bands plotted for the 10th cycle) for both subfigures in the well-mixed case: (a) mean value, (b) confidence band.

tively. Only one repetition of the simulation run was performed, and the confidence bands were obtained using Eq. (11).

Figs. 4 and 5 summarize the simulated results for the partially mixed and well-mixed systems, respectively. The figures demonstrate that introducing the down-sampling strategy into the SRM-DI does not significantly reduce the accuracy of the simulation. The simulated results obtained with the down-sampling factors 3 and 5 were nearly within the confidence band determined with $M = 1$ (i.e., the base case). However, when M was increased, e.g., $M = 9.3$, the profiles of scalar variables overlapped with the confidence bands of the corresponding variables for the base case. Therefore, overall it can be concluded that the down-sampling procedure is acceptable in the simulation of a HCCI engine under given conditions, although larger down-sampling factors can lead to higher error.

Furthermore, the computational costs with and without down-sampling are compared and the results are listed in Table 4. It can be seen that within acceptable error, introducing down-sampling can speed up the simulation approximately eight times for both partially mixed and well-mixed systems.

Following the systematic numerical investigations, the model was validated against experimental data for combustion parameters and emissions, as given in the next section.

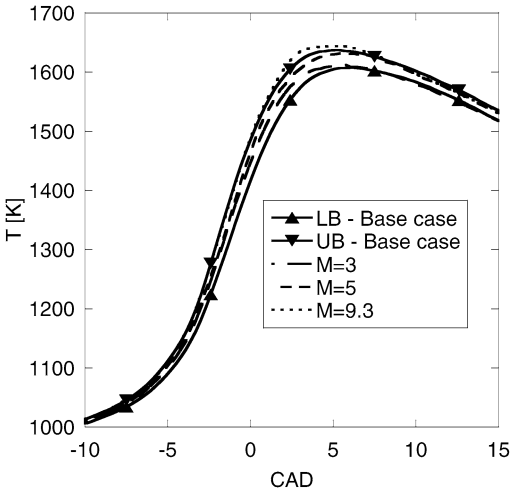

(a) In-cylinder temperature

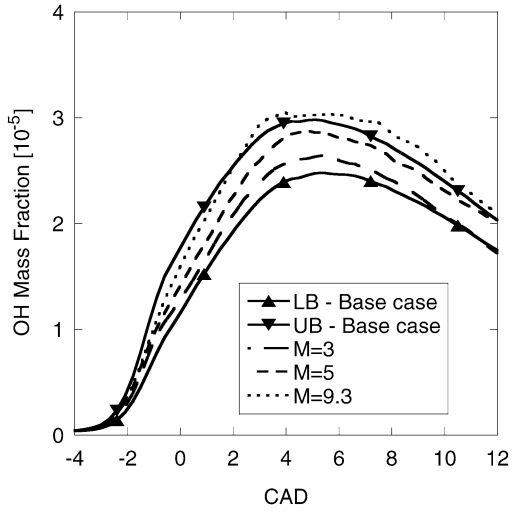

(b) OH mass fraction

Fig. 4. Effect of down-sampling on the simulated properties of the gas mixture in the well-mixed case ($\tau_m = 2.0 \times 10^{-4}$ s): (a) in-cylinder temperature, (b) OH mass fraction.

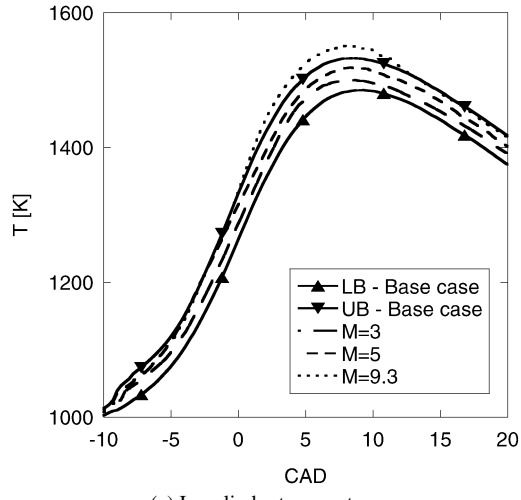

(a) In-cylinder temperature

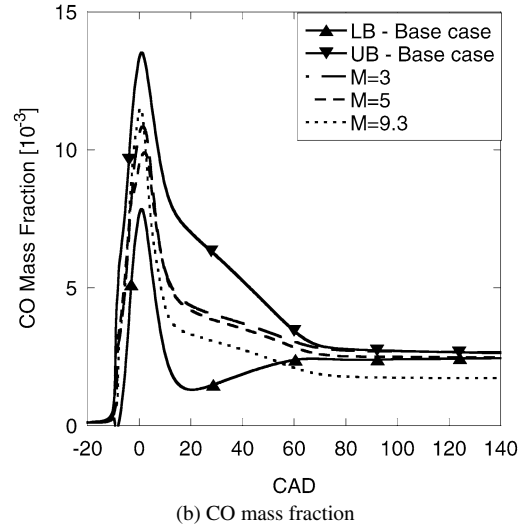

(b) CO mass fraction

Fig. 5. Effect of the down-sampling on the simulated properties of the gas mixture in the partially mixed case ($\tau_m = 2.0 \times 10^{-2}$ s): (a) in-cylinder temperature, (b) CO mass fraction.

5. Model validation

Measurements for in-cylinder pressure and CO, HC, and NO_x emissions were carried out on the same engine as described in Section 4, but with different set of operating conditions. The operating parameters are given in Table 5.

Table 4
Comparison of computational times for well-mixed and partially mixed systems

Simulation case	Factor M	CPU time (min)	
		$\tau_m = 2 \times 10^{-2}$ s	$\tau_m = 2 \times 10^{-4}$ s
Base case ($N = n = 334$)	1	705	252
Down-sampling ($n = 111$)	3	237	86
Down-sampling ($n = 66$)	5	138	47
Down-sampling ($n = 36$)	9.3	83	30

Table 5
Engine operating parameters

Description	Value	Units
Speed	1600	RPM
Fuel	Gasoline-92	–
EVO/EVC	132/205 ATDC	CAD
IVO/IVC	155/224 ATDC	CAD
SOI/EOI	190/205 ATDC	CAD
EGR ratio	36%	–
Relative air/fuel ratio	1.36	–

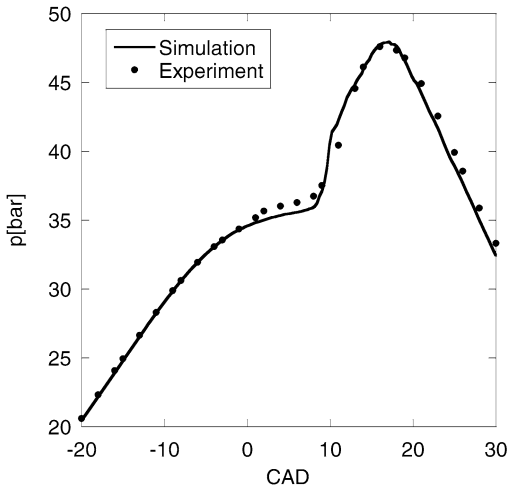

Fig. 6. Experimental and simulated in-cylinder pressure profiles for a two-stroke HCCI engine ($\lambda = 1.36$, 1600 RPM).

HCCI combustion with too advanced an autoignition timing can result in a rapid surge in NO_x emissions and harsh noise caused due to high pressure-rise rates. By delaying the autoignition timing, NO_x and noise can be controlled with only a slight sacrifice of the thermal efficiency. This section presents a comparison between model predictions and measurements for an operating condition corresponding to the autoignition timing delayed after TDC.

The same reaction mechanism with isooctane (mass fraction 0.9181) and n-heptane (mass fraction 0.0819) was used to correspond to an octane number of 92 (RON = 92). A turbulent mixing time, $\tau = 6 \times 10^{-3}$ [s] was implemented for the closed volume portion of the engine cycle. The number of stochastic particles was chosen as $N = 100$, and the parameters C_h and T_w were set to 40 and 450 K, respectively. The results of the model validation are shown in Figs. 6 and 7. The model agrees well with the experimental data for the in-cylinder pressure profile as well as for the CO emissions; however, the unburnt HC and NO_x emissions are underpredicted. Prediction of unburnt HC emissions can be further improved by accounting for crevices, as most of the HCs originate from crevices for an engine operating in the premixed mode. In the experiments, a significant cycle-to-cycle variation for the peak in-cylinder pressure (hence the temperature) was observed. In such a scenario, the engine cycles corresponding to higher peak temperatures were found to be responsible for appreciable levels of NO_x emissions. Cycle-to-cycle variations have not been accounted for within the present work.

In the next section, the model is utilized to predict the effect of varying engine operating parameters on HCCI combustion and emissions.

6. Effects of relative air–fuel ratio and injection timing on combustion

In order to control HCCI engine operation, several approaches have been investigated, for example, changing relative air–fuel ratio, injection timing, IVO

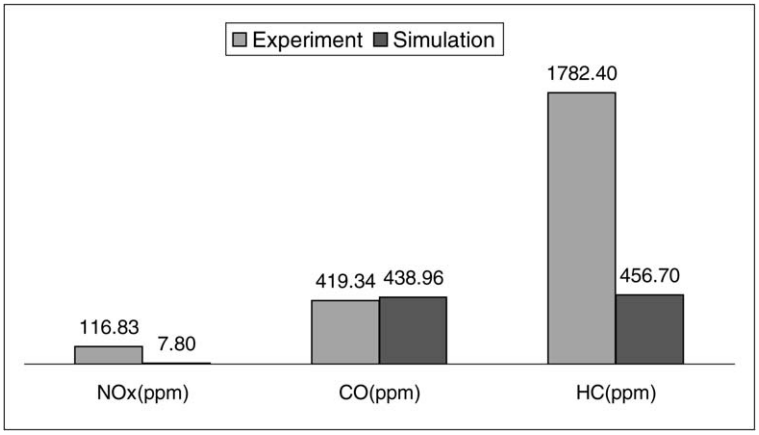

Fig. 7. Comparison of model predictions and measurements for CO, HC, and NO_x emissions from a two-stroke HCCI engine ($\lambda = 1.36$, 1600 RPM).

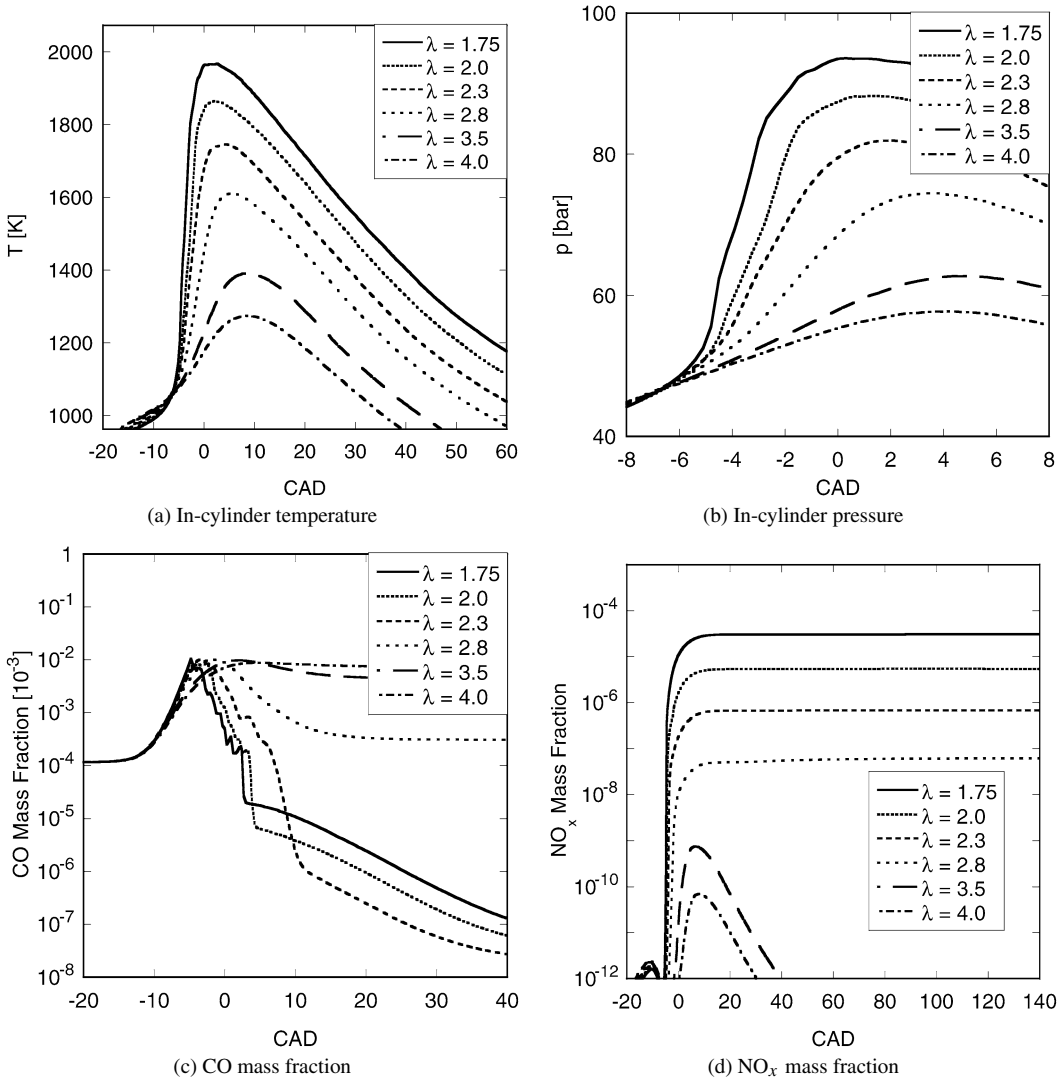

(a) In-cylinder temperature (b) In-cylinder pressure

(c) CO mass fraction (d) NO_x mass fraction

Fig. 8. Effect of the relative air–fuel ratio on the mixture's properties in the well-mixed case (1200 RPM): (a) in-cylinder temperature, (b) in-cylinder pressure, (c) CO mass fraction, (d) NO_x mass fraction.

timing, EVC timing, engine speed, boost pressure, and intake gas temperature, as well as hybrid methods involving the integration of these strategies. With the current development of the SRM-DI model, not all mentioned strategies can be investigated in this work. Here, we focus on evaluating the effect of two specific engine strategies, namely, varying relative air–fuel ratio and early direct injection timing. Based on the volume-averaged mixing time obtained from CFD calculations, the well-mixed case was chosen and the influence of varying the aforementioned engine operating parameters on combustion parameters and emissions was predicted and qualitatively compared with experimental results reported in literature. For all the studies, we used the same engine as described in Section 4.

6.1. Relative air–fuel ratio

HCCI combustion is influenced by the temperature, the pressure, and the species mass fractions of the air–fuel–EGR mixture in the cylinder. Varying the relative air–fuel ratio (λ) directly influences the fuel concentration. Generally, this technique is integrated with others such as injection timing, injection method, and variable valve timing to control the HCCI engine.

In this section, HCCI combustion with early single-stage direct injection was investigated while relative air–fuel ratio was varied from 1.75 to 4.0. The results are shown in Fig. 8. It can be observed that as λ decreases, the peak temperature, the peak pressure, the mass fraction of NO_x increase while CO mass fraction decreases. When λ equals 1.75, the maxi-

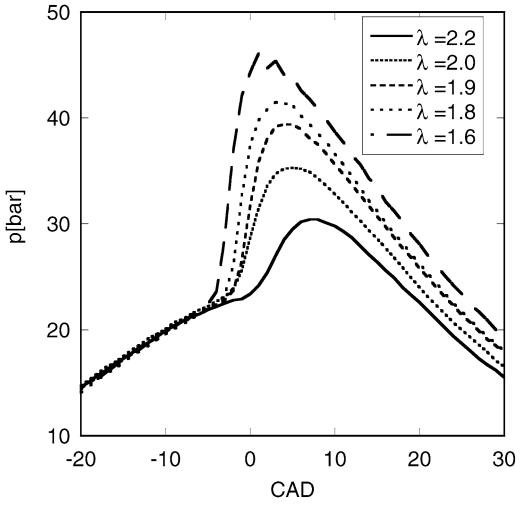

Fig. 9. Effect of relative air–fuel ratio on cylinder pressures and heat release rate with single injection and injection timing = 100° ATDC in intake stroke (1000 RPM; Ref. [28]).

mum pressure gradient is higher than 15 bar/CAD. This could cause engine knock and high NO_x emissions. On the other hand, when λ is too high, i.e., fuel is too lean, the mixture fails to burn completely, in turn leading to high CO concentration. The trends associated with the influence of varying λ on the in-cylinder pressure match well with the experimental data in Fig. 9 (Fig. 7 of Ref. [28]). In particular, for the experimental data, it can be observed that the ignition timing varies with λ, on account of the steady state operation. Whereas, for the numerical study, all simulations begin from the same initial condition for the first of the two-cycle simulation.

6.2. Direct injection timing

In this section, the effect of varying SOI is studied. As the injection is well before TDC, the mixture is almost homogeneous before the ignition is triggered. Fig. 10a depicts the influence of early direct injection timing on the combustion parameters, namely, autoignition timing (crank angle corresponding to 10% cumulative burn rate) and combustion duration (difference between the crank angles corresponding to 90% and 10% burnt fractions), as predicted by the model. It can be observed that the two combustion parameters show hardly any sensitivity to the range of early injection timings studied. This behavior can be attributed to the appreciable time (following early direct injection) available until the end of the compression stroke for the air, the fuel, and the EGR to mix almost homogeneously. Qualitatively this is supported through measurements (as shown in Fig. 10b)

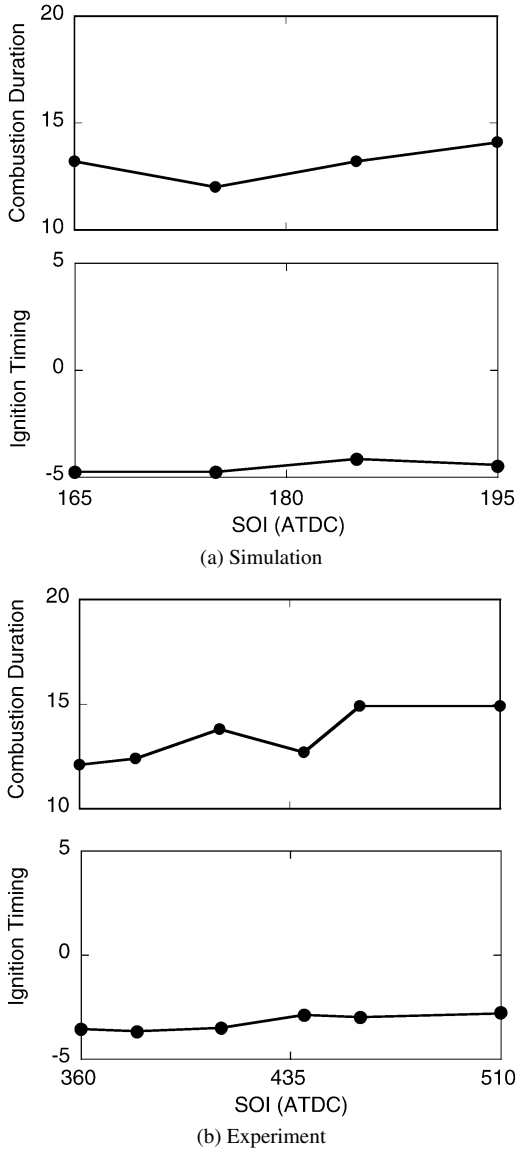

(a) Simulation

(b) Experiment

Fig. 10. Effect of injection timing on HCCI combustion varying with SOI: (a) simulation (λ = 2.8, 1200 RPM); (b) experiment (λ = 1.2, 1800 RPM) (Ref. [28]).

carried out on a four-stroke gasoline-fueled HCCI engine elsewhere, where the effect of early direct injection timing on HCCI combustion was reported to be negligible. To study the effect of direct injection timings later than those studied above, a more sophisticated treatment of the mixing (than what the IEM model provides) is necessary. In particular, localness of the scalars and stratification need to be accounted for, which is the subject of the next publication.

However, for the given conditions the new SRM-DI model qualitatively predicted the effects of varia-

tion in the relative air–fuel ratio and the early direct injection timing on HCCI combustion and emissions.

7. Conclusions

A novel SRM-DI model based on the probability density function (PDF) approach was formulated to simulate early direct injection HCCI engine operation. With the incorporation of the gas exchange processes, the computational expense increased rapidly. Hence, a conservative down-sampling procedure combined with a weighted-particle Monte Carlo method was developed to reduce the number of particles while conserving the statistical properties of the ensemble.

A systematic numerical investigation of the model performance with respect to the various numerical parameters was carried out. It was observed that the algorithm was more sensitive to the number of particles than to the number of conserved chemical species. Furthermore, multiple cycle simulation studies demonstrated that the error due to down-sampling was not accumulated with respect to the number of engine cycles. Additionally, implementing the down-sampling technique in an engine cycle simulation resulted in a speed-up by a factor of 8, without incurring significant error in the numerical solution.

The model validation shows that the predictions for in-cylinder pressure and CO emissions at a single operating point in a two-stroke direct injection HCCI engine agree well with the experimental values. This depicts the model's ability to make quantitative predictions on HCCI combustion and emissions, for the given conditions.

Furthermore, the influence of varying the relative air–fuel ratio and direct injection timing on HCCI combustion parameters as depicted by the model agreed well in terms of qualitative trends observed in measurements elsewhere.

The work presented in this paper was only focused on early direct injection; however, the framework built here can now be used to formulate an advanced model for simulating multiple and late direct injection HCCI combustion. Currently efforts are being focused on developing detailed submodels for spray injection and turbulent mixing to improve the predictive power of the model.

Acknowledgments

We express our sincere thanks to Toyota Motor Co., Japan, for providing financial support for the research work. HS and AB are grateful to the Centre for Scientific Enterprise Limited (CSEL) for the fellowship funding. Thanks are due to our colleagues at the Computational Modelling Group, University of Cambridge, for their help with the manuscript.

References

[1] F. Zhao, T. Asmus, D. Assanis, J. Dec, J. Eng, P. Najt, Homogeneous Charge Compression Ignition (HCCI) Engines Key Research and Development Issues, Society of Automotive Engineers, U.S., 2003.
[2] T. Urushihara, K. Hiraya, A. Kakuhou, T. Itoh, SAE paper, No. 2003-01-0749 (2003).
[3] R. Standing, N. Kalian, T. Ma, H. Zhao, M. Wirth, A. Schamel, SAE paper, No. 2005-01-0132 (2005).
[4] M. Guenthner, W. Sauter, F. Schwarz, A. Velji, U. Spicher, A study of the ignition and combustion process in a gasoline HCCI engine using port and direct fuel injection, in: 6th International Symposium on Diagnostics and Modeling of Combustion in Internal Combustion Engines (COMODIA), 2004, Yokohama, Japan.
[5] B. Leach, H. Zhao, Y. Li, T. Ma, SAE paper, No. 2005-01-0134 (2005).
[6] R. Hasegawa, H. Yanagihara, SAE paper, No. 2003-01-0745 (2003).
[7] F. Tao, Y. Liu, B.H. RempelEwert, D. Foster, R.D. Reitz, D. Choi, P.C. Miles, SAE paper, No. 2005-01-0121 (2005).
[8] Y. Ra, R.D. Reitz, SAE paper, No. 2005-01-0148 (2005).
[9] G. Lechner, T. Jacobs, C. Chryssakis, D. Assanis, R. Siewert, SAE paper, No. 2005-01-0167 (2005).
[10] Y. Nishijima, Y. Asaumi, Y. Aoyagi, SAE paper, No. 2002-01-0109 (2002).
[11] T. Tomoda, M. Kubota, R. Shimizu, Y. Nomura, Numerical analysis of mixture formation of a direct injection gasoline engine, in: 5th International Symposium on Diagnostics and Modeling of Combustion in Internal Combustion Engines (COMODIA), 2001, Nagoya, Japan.
[12] W. Su, H. Wang, B. Liu, SAE paper, No. 2005-01-0117 (2005).
[13] K. Narayanaswamy, C.J. Rutland, SAE paper, No. 2004-01-2997 (2004).
[14] K. Narayanaswamy, R. Hessel, C.J. Rutland, SAE paper, No. 2005-01-3743 (2005).
[15] R. Jhavar, J. Christopher, SAE paper, No. 2003-01-0154 (2003).
[16] M. Kraft, P. Maigaard, F. Mauss, M. Christensen, B. Johansson, Proc. Combust. Inst. 28 (2000) 1195–1201.
[17] P. Maigaard, F. Mauss, M. Kraft, J. Eng. Gas Turbines Power 125 (2003) 230–466.
[18] A. Bhave, M. Balthasar, M. Kraft, F. Mauss, Int. J. Engine Res. 5 (1) (2004) 93–103.
[19] A. Bhave, M. Kraft, L. Montorsi, F. Mauss, SAE paper, No. 2004-01-0561 (2004).
[20] A. Bhave, M. Kraft, F. Mauss, A. Oakley, H. Zhao, SAE paper, No. 2005-01-0161 (2005).

[21] A. Vikhansky, M. Kraft, J. Comput. Phys. 203 (2005) 371–378.
[22] S.M. Correa, M.E. Braaten, Combust. Flame 94 (1993) 469–486.
[23] J.Y. Chen, Combust. Sci. Technol. 122 (1997) 63–94.
[24] A. Bhave, M. Kraft, SIAM J. Sci. Comput. 25 (5) (2004) 1798–1823.
[25] S.B. Pope, Prog. Energy Combust. Sci. 11 (1985) 119–192.
[26] G. Strang, SIAM J. Numer. Anal. 5 (3) (1968) 506–517.
[27] B. Yang, S.B. Pope, Combust. Flame 112 (1998) 16–32.
[28] Z. Wang, J. Wang, S. Shuai, Q. Ma, SAE paper, No. 2005-01-0137 (2005).